communications materials

Article

https://doi.org/10.1038/s43246-024-00617-x

Anomalous Nernst effect in the noncollinear antiferromagnet Mn_5Si_3

Christoph Sürgers [1] ✉, Gerda Fischer [1], Warlley H. Campos [2], Anna Birk Hellenes[2], Libor Šmejkal[2,3], Jairo Sinova[2], Michael Merz [4,5], Thomas Wolf[5] & Wolfgang Wernsdorfer[1,5]

Investigating the off-diagonal components of the conductivity and thermoelectric tensor of materials hosting complex antiferromagnetic structures has become a viable method to reveal the effects of topology and chirality on the electronic transport in these systems. In this respect, Mn_5Si_3 is an interesting metallic compound that exhibits several antiferromagnetic phases below 100 K with different collinear and noncollinear arrangements of Mn magnetic moments determined from neutron scattering. Previous electronic transport measurements have shown that the transitions between the various phases give rise to large changes of the anomalous Hall effect. Here, we report measurements of the anomalous Nernst effect of Mn_5Si_3 single crystals that also show clear transitions between the different magnetic phases. In the noncollinear phase, we observe an unusual sign change of the zero-field Nernst signal with a concomitant decrease of the Hall signal and a gradual reduction of the remanent magnetization. Furthermore, a symmetry analysis of the proposed magnetic structures shows that both effects should actually vanish. These results indicate a symmetry-breaking modification of the magnetic state with a rearrangement of the magnetic moments at low temperatures, thus questioning the previously reported models for the noncollinear magnetic structure obtained from neutron scattering.

Antiferromagnetic materials have attained a renaissance in condensed-matter research due to technical advantages like low stray-fields and ultrafast switching compared to ferromagnets, leading to the development of a new field coined antiferromagnetic spintronics[1,2]. A particular class of materials is antiferromagnets in which the magnetic moments of atoms are ordered in a noncollinear fashion. They often exhibit a nonzero Berry curvature leading to an emergent electromagnetic response, which can be harnessed for practical purposes[3–6]. In noncollinear antiferromagnets and spin liquids, a nonzero Berry curvature gives rise to an unusually large anomalous Hall effect (AHE)[7–11]. Like in ferromagnets, the intrinsic part of the AHE is obtained by integration of the Berry curvature of occupied electronic bands over the entire Brillouin zone[12,13]. Similar to the AHE, its thermoelectric counterpart, the anomalous Nernst effect (ANE), generates a voltage transverse to the heat flow and magnetization. This transverse thermopower provides a measure of the Berry curvature only at the Fermi energy E_F[12,13]. It is therefore not a priori clear that a large AHE guarantees a large ANE.

The AHE and ANE have been the subject of intense research and development in recent years and hold great promise for practical applications in the fields of spintronics and thermoelectronics. Both effects can be extraordinary large in chiral antiferromagnets like Mn_3Sn[7,10,14] and Mn_3Ge[8,9,11,15,16] despite their tiny magnetization. Here, the enhanced Berry-phase curvature is associated with the existence of Weyl points near the Fermi level where the Berry curvature diverges. In addition to the thermoelectric ANE, a sizeable thermal Hall effect (Righi-Leduc effect) generated by the Berry curvature has been reported for these two materials[10,11].

The intermetallic compound Mn_5Si_3 is a noncollinear antiferromagnet that has gained attention due to unusual thermodynamic and electronic transport phenomena[17–22]. Mn_5Si_3 has a hexagonal crystal structure (space group $P6_3/mcm$) with two inequivalent Mn lattice sites Mn_1 and Mn_2 at room temperature and undergoes two structural phase transitions toward orthorhombic symmetry below 100 K.

Figure 1 shows the magnetic phase diagram of Mn_5Si_3 in a magnetic field H oriented along the crystallographic c axis. Various methods including

[1]Physikalisches Institut, Karlsruhe Institute of Technology, Kaiserstraße 12, 76131 Karlsruhe, Germany. [2]Institut für Physik, Johannes Gutenberg Universität Mainz, Mainz, Germany. [3]Institute of Physics, Czech Academy of Sciences, Praha 6, Czech Republic. [4]Karlsruhe Nano Micro Facility (KNMFi), Karlsruhe Institute of Technology, Karlsruhe, Germany. [5]Institute for Quantum Materials and Technologies, Karlsruhe Institute of Technology, Kaiserstraße 12, 76131 Karlsruhe, Germany. ✉e-mail: christoph.suergers@kit.edu

neutron scattering have confirmed the existence of an antiferromagnetic phase AF2 between the Néel temperatures T_{N1} = 60 K and T_{N2} = 100 K with zero Mn_1 moments and a collinear arrangement of two-thirds of Mn_2 moments with opposite orientations on adjacent sites of the orthorhombic structure [Fig. 2a][17,21,23–25].

In the antiferromagnetic AF1 phase below T_{N1} = 60 K, a highly non-collinear and noncoplanar arrangement of magnetic moments is observed where the Mn_1 atoms also acquire a magnetic moment in addition to the two thirds of Mn_2 moments, although the details of the size and orientation of the Mn moments are still under dispute[26–28], see Fig. 2b, c. The noncollinearity results from the combined effects of magnetic frustration and anisotropy.

Inelastic neutron-scattering measurements of the low-energy dynamics reveal a single-anisotropy energy gap in the AF1 phase and a double gap in the AF2 phase arising from a bi-axial anisotropy[28,29]. Concomitantly performed density-functional theory calculations indicate that in the AF1 phase the crystallographic *b* axis is the easy axis, whereas in the AF2 phase the *b* and *c* axes are the first and second preferred magnetic easy axes, respectively, and *a* is the hard axis[30].

As soon as the magnetic structure changes from collinear AF2 to noncollinear AF1 below T_{N1} = 60 K, a strong AHE is observed[18–20]. In addition, the existence of a magnetic-field induced intermediate phase AF1' has been inferred from neutron scattering and electronic transport measurements[20,21,25]. Finally, at high magnetic fields, a collinear phase with similar properties to the zero-field AF2 phase is stabilized[18,20,21,28]. We mention that an additional phase has been reported to exist in single crystals grown out of Cu flux which was attributed to strain or stress introduced by Cu inclusions from the crystal growth[31]. It is these different magnetic moment configurations of noncollinear and collinear order achieved at different magnetic fields and temperatures, that make the Mn_5Si_3 compound so interesting for investigations of the effect of topology and complex magnetic order on the magnetotransport properties.

For the noncollinear AF1 phase, previous first-principle calculations assumed a Heisenberg Hamiltonian that takes into account magnetic exchange and biaxial anisotropy[29]. Through modeling of the low-temperature spin-wave spectrum obtained by inelastinc neutron scattering at 10 K, two additional exchange constants representing the Mn_1-Mn_1 and Mn_1-Mn_2 interactions have been proposed by Biniskos et al.[28], resulting in a ground-state spin arrangement in the AF1 phase that is different from the previous AF1 phase reported by Brown et al.[26]. Here, in zero magnetic fields the Mn_1 atoms carry a magnetic moment oriented along the orthorhombic *b* axis while the two-thirds of Mn_2 atoms carry a magnetic moment with a significant component along the *c* axis, respectively (Fig. 2c).

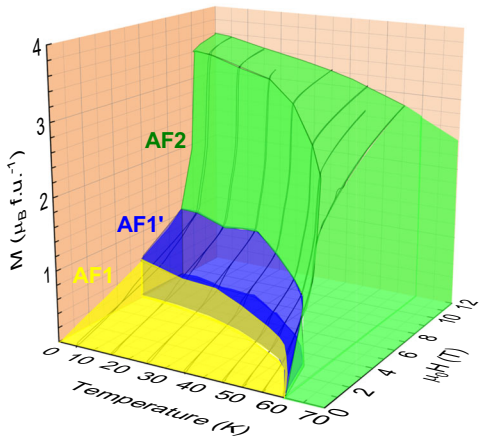

Fig. 1 | Magnetic phases of Mn_5Si_3. Magnetic phase diagram and magnetic moment obtained from individual magnetization curves, see Fig. 3a. AF1 and AF1' exhibit noncollinear antiferromagnetic structures while AF2 is a collinear antiferromagnetic phase.

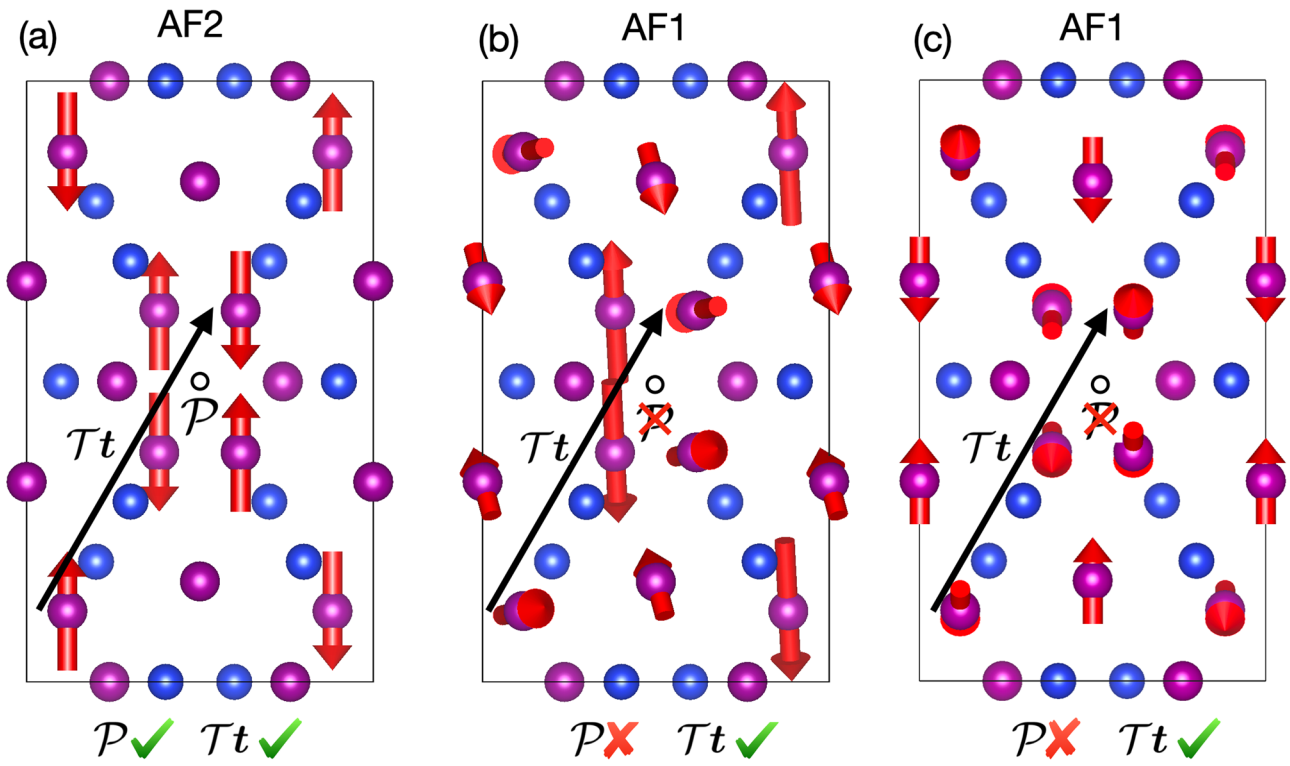

Fig. 2 | Magnetic structures of Mn_5Si_3. Crystal structures of the low-temperature (T < 100 K) antiferromagnetic phases in the orthorhombic *a*-*b* plane indicated by the black outlined rectangle ($b > a$). Mn and Si atoms are shown in magenta and blue color, respectively. Red arrows indicate different Mn magnetic moments. **a** Collinear AF2 phase observed for 60 K < T < 100 K[17,24,29,56]. **b** Noncoplanar AF1 phase without inversion symmetry proposed in ref. 26 for T < 60 K[56]. **c** Illustration of the AF1 phase proposed in ref. 28 for T < 60 K, also noncoplanar and noncentrosymmetric.

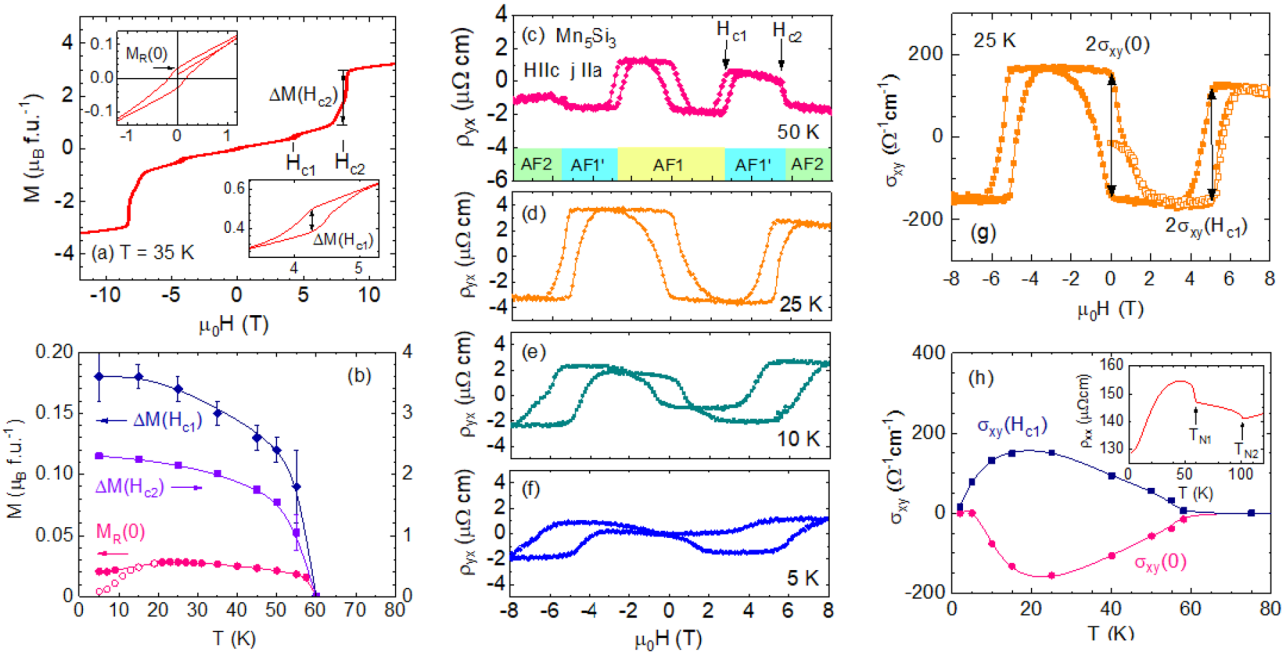

Fig. 3 | Magnetization and anomalous Hall effect of Mn_5Si_3. a Magnetization $M(H)$ at $T = 35$ K. Insets show a close up of $M(H)$ near zero field and around the transition at H_{c1}. **b** Remanent field $M_R(0)$ and magnetization jumps $\Delta M(H_{c1})$ and $\Delta M(H_{c2})$ obtained from $M(H)$ vs temperature. Closed (open) circles indicate data obtained after applying a magnetic field of ± 5 T (± 2 T) before measuring $M_R(0)$. The accuracy with which the values from $M(H)$ loops could be determined is indicated by error bars. **c**–**f** Anomalous Hall effect for various temperatures. **g** Anomalous Hall conductivity $\sigma_{xy}(H)$ at $T = 25$ K. Open symbols represent data in the virgin magnetic state before sweeping the field from zero to +8 T. **h** Temperature dependence of $\sigma_{xy}(0)$ and $\sigma_{xy}(H_{c1})$. Inset shows the resistivity $\rho_{xx}(T)$ with indicated Néel temperatures T_{N1} and T_{N2} at the magnetic phase transitions AF1/AF1' and AF1'/AF2, respectively. The magnetic field was always oriented along the crystallographic c axis.

Furthermore, the field-induced phase transition between AF1 and AF1' was simulated by including a Zeeman term in the Heisenberg Hamiltonian[28]. In this model, it is assumed that the Mn_1 moments are longitudinally susceptible, i.e., their size is affected by an external field. Starting from the proposed ground state (Fig. 2c) and increasing the magnetic field applied along the c axis, a "spin flop" phase with coplanar Mn_2 moments in the a-b plane is succeeded by an AF1'-like phase, where the Mn_1 moments are also predominantly orientated in the a-b plane, but start to have a component along the c axis. At even higher fields, a transition to a field-induced phase is proposed, with collinear and antiparallel oriented Mn_2 moments along the b axis and nonvanishing Mn_1 moments aligned parallel to the direction of the magnetic field. All models for the magnetic structure reported so far suggest that the field-induced phase at high magnetic fields has similar properties as the zero-field AF2 phase, although it is not clear whether the Mn_1 moment eventually collapses or not[25,28].

In addition to single crystals, thin epitaxially strained Mn_5Si_3 layers have been grown that exhibit collinear order up to higher temperatures and a spontaneous AHE due to the breaking of time-reversal symmetry by an unconventional staggered spin-momentum interaction[32]. In the ideal case considered by theory, the zero net magnetization allows for a non-relativistic electronic structure with altermagnetic collinear spin polarization in momentum space[33,34]. This gives rise to anomalous Hall and Nernst effects experimentally observed in thin epitaxial Mn_5Si_3 films with a small net magnetization of 20 - 60 mμ_B/f.u.[35]. Recently, spin-orbit torque switching of the Néel vector has been demonstrated for strained Mn_5Si_3 films and a strong enhancement of the ANE upon Mn doping of a Mn_5Si_3 film has been attributed to the shift of the Fermi level[36,37].

The observation of a nonzero AHE and its strong changes at the magnetic phase boundaries, the link between the AHE and ANE via the Berry-phase concept, and the hitherto reports of both effects observed in other noncollinear antiferromagnets, motivated this study of the ANE in Mn_5Si_3, where we focus on the noncollinear magnetic phase at low temperatures.

Results

Magnetization and anomalous Hall effect

Figure 3a shows a typical magnetization curve of Mn_5Si_3 at $T = 35$ K with the magnetic field applied parallel to the crystallographic c axis. The two jumps of the magnetization $\Delta M(H_{c1})$ and $\Delta M(H_{c2})$ at magnetic fields H_{c1} and H_{c2}, respectively, are attributed to the AF1/AF1' and AF1'/AF2 phase transitions. Before sweeping the magnetic field, the sample has a magnetization much lower than the remanent magnetization $M_R(0)$, see left inset Fig. 3a. This indicates that the antiferromagnetic structure is not fully compensated in the magnetically pristine state and exhibits weak moments that allow the domain configuration to be changed by applying a magnetic field and generate a net magnetization along the field direction. The hysteresis around zero field is not observed when the magnetic field is oriented perpendicularly to the c axis for all temperatures below 60 K[19]. The heights of the jumps are plotted in Fig. 3b together with the remanent magnetization $M_R(0)$ vs. temperature. A remarkable detail is the decrease of $M_R(0)$ when cooling below 20 K while $\Delta M(H_{c1})$ and $\Delta M(H_{c2})$ continuously increase with decreasing temperature below $T_{N1} = 60$ K. Moreover, the absolute value of $M_R(0)$ below 20 K depends on the maximum applied magnetic field, i.e. ± 2 T or ± 5 T, see Fig. 3b, indicating either a reformation of antiferromagnetic domains with opposite Néel vectors in this temperature range[32] or a modification of the local magnetic structure. Magnetic polarization at fields larger than 5 T was not possible without entering the AF1' phase.

The phase transitions are clearly observed in the AHE of Mn_5Si_3, see Fig. 3c–f. At 50 K, below T_{N1}, the AHE strongly changes around zero field and at magnetic fields H_{c1} and H_{c2}. In the collinear AF2 phase the AHE vanishes[20]. The absolute value of the transverse resistivity $\rho_{yx}(0)$ in the remanent state at zero field, i.e., after completing a full magnetic field cycle, increases with decreasing temperature down to 25 K and then decreases and even vanishes at $T = 5$ K while $M_R(0)$ remains nonzero.

Figure 3g shows the Hall conductivity $\sigma_{xy} = \rho_{yx}/(\rho_{xx}^2 + \rho_{yx}^2)$, where ρ_{xx} is the longitudinal resistivity, see inset Fig. 3h. In the magnetically virgin state before sweeping the magnetic field, σ_{xy} is very small compared to the

remanent state $\sigma_{xy}(0)$ observed after completion of a field sweep to high fields, similar to the magnetization $M(H)$, Fig. 3a. A strong difference between the temperature dependences of $\rho_{yx}(0)$ was already reported earlier when the sample was cooled down in zero field from above T_{N1} and subsequently polarized in a magnetic field of $\pm$ 3 T[20].

σ_{xy} is affected by extrinsic contributions arising from skew scattering or side-jump mechanism and by the intrinsic Berry-phase contribution[3]. In the dirty and ultraclean regimes of electron scattering the dependence of σ_{xy} on the longitudinal conductivity σ_{xx} can be described by a power law $\sigma_{xy} \propto \sigma_{xx}^{\alpha}$ with $\alpha > 0$. In the intermediate regime of moderate conductvity $3 \times 10^3 - 5 \times 10^5\ \Omega^{-1}\mathrm{cm}^{-1}$ the AHE is predominated by the intrinsic Berry-phase contribution where σ_{xy} is independent of σ_{xx}[38,39]. In the present case, the single crystals with $\sigma_{xy} = 150\ \Omega^{-1}\mathrm{cm}^{-1}$ and $\sigma_{xx} = 7400\ \Omega^{-1}\mathrm{cm}^{-1}$ fall just within this intermediate regime as discussed earlier[20,40], similar to the noncollinear antiferromagnets Mn_3Ge and Mn_3Sn[41]. From $\rho_{xx} = 135\ \mu\Omega$cm, a Fermi velocity $v_F = 2 \times 10^6$ m/s[42], and an electron density $n = 1 \times 10^{22}\ \mathrm{cm}^{-3}$[20] we estimate an electron mean free-path of 5.2 nm, larger than several lattice parameters, supporting the classification of this material as a moderately conductive metal.

The absolute values of the remanent $\sigma_{xy}(0)$ and $\sigma_{xy}(H_{c1})$ plotted in Fig. 3h gradually increase between $T_{N1} = 60$ K and ≈ 25 K but then drop to very low values for $T \leq 20$ K. We emphasize that $\sigma_{xy}(0)$ completely vanishes for $T \leq 5$ K while $\sigma_{xy}(H_{c1})$ remains at a low value of 17 $\Omega^{-1}\mathrm{cm}^{-1}$ at $T = 2$ K. The decrease of the AHE toward low temperatures is unusual for a well established magnetic order but could arise from domain reformation around zero field mentioned above. However, the fact that both contributions to the AHE, $\sigma_{xy}(0)$ and $\sigma_{xy}(H_{c1})$, decrease toward zero temperature while the magnetization $\Delta M(H_{c1})$ remains constant, demonstrates that a different mechanism might be at hand. For antiferromagnetic Mn_3Sn, a sharp drop of σ_{zx} and σ_{yz} in connection with a strong increase of $|\sigma_{xy}|$ was observed in the low temperature spin-glass phase below 50 K, where a large ferromagnetic compound evolves due to spin canting[7,41]. This suggests that in Mn_5Si_3 the magnetic moments possibly rearrange at low temperatures as previously inferred from analyzing the evolution of spin-wave energies, revealing another field induced phase-transition below the AF1/AF1' phase boundary[28].

Anomalous Nernst effect

In the following we focus on the ANE obtained on the same Mn_5Si_3 single crystal. Theoretically, the ANE generates an electric field $\mathbf{E} = Q_S \mu_0 \mathbf{M} \times (-\nabla T)$ perpendicular to the directions of the magnetization $\mathbf{M}$ and temperature gradient $-\nabla T$, where Q_S is the anomalous Nernst coefficient and μ_0 is the magnetic permeability of free space. Figure 4c shows a cartoon of the ANE setup. For the present configuration with H_z parallel to the crystallographic c axis, $|\mathbf{M}| = M_z$, and with a temperature gradient along x, this simplifies to $E_y = -S_{yx} \nabla T_x$, with $S_{yx} = Q_S \mu_0 M_z$.

The Nernst signal S_{yx} is experimentally measured by

$$S_{yx} = \frac{\Delta V_y\, l_x}{\Delta T_x\, l_y} \tag{1}$$

where we made use of the fact that $E_y = -\Delta V_y / l_y$ and $\nabla T_x = \Delta T_x / l_x$.

Figure 5a–d shows S_{yx} vs magnetic field H applied parallel to the c direction and heat flow along the b direction for different temperatures below T_{N1}. At 50 K, the transitions between the different magnetic phases are observed as clear changes of S_{yx} with a hysteresis, very similar to the behavior of the AHE [Fig. 3c–f].

S_{yx} is zero in the collinear AF2 phase for temperatures $T > 60$ K, see Fig. 6, concomitant with a vanishing AHE and magnetization. Again, after reaching a maximum the magnitude of S_{yx} decreases with decreasing temperature below 25 K, similar to the behavior of the AHE, *cf.* Fig. 3c–f. In addition, the coercive fields of $M(H)$, ρ_{yx}, and S_{yx} around zero magnetic field are of similar size and continuously decrease from 15 K to 60 K as previously observed for $\rho_{yx}(T)$[20]. This indicates that the effects of the magnetic field on ρ_{yx} and S_{yx} are of similar origin.

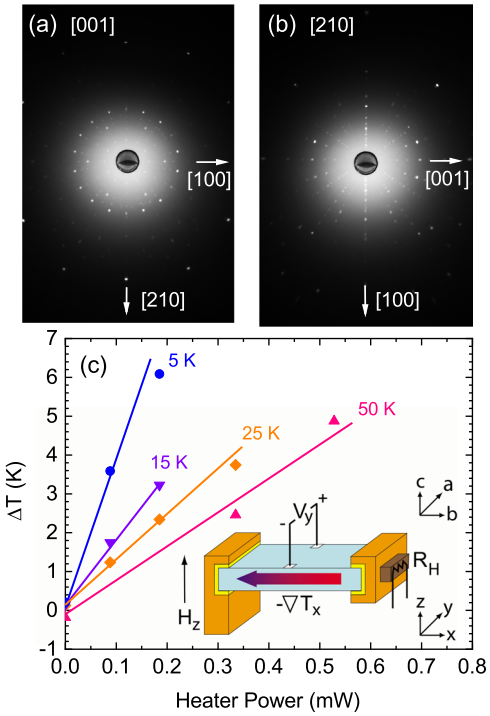

Fig. 4 | Characterization of Mn_5Si_3 single crystals. Laue diffraction patterns of a Mn_5Si_3 single crystal oriented with the x-ray beam along the **a** [001] and **b** [210] directions of the hexagonal structure at room temperature. At $T < 100$ K, the [100], [210], and [001] directions correspond to the *a*, *b*, and *c* axes, respectively, of the orthorhombic phase. **c** Temperature difference $\Delta T = T_h - T_c$ between the hot and the cold end of the sample vs heater power for different average temperatures T_0. Solid lines indicate a linear behavior. Inset shows a cartoon of the experimental set up and the orientation of the sample with crystallographic axes *a*, *b*, and *c* of low-temperature orthorhombic phase with respect to the sample holder.

A remarkable difference is the sign change of the remanent $S_{yx}(0)$ below 25 K [see Fig. 5b, c] before it vanishes at lower temperatures. This behavior is also observed on another single crystal for H applied parallel to the c direction and heat flow along the a direction but not for H applied parallel to the a or b directions where no AHE appeared at zero field[20], see Fig. 6.

The temperature dependence is seen more clearly in plots of $S_{yx}(0, T)$ and $S_{yx}(H_{c1}, T)$, Fig. 5e. Whereas $\sigma_{xy}(0)$ (in phase AF1) and $\sigma_{xy}(H_{c1})$ (in phase AF1') have opposite signs but are of the same magnitude [Fig. 3h], $S_{yx}(0)$ also has the opposite sign of $S_{yx}(H_{c1})$ but only reaches half of its value. Both effects, AHE and ANE, do not scale with the change of the magnetization at zero field and at H_{c1}, confirming that they arise from topology and from the intrinsic Berry-curvature effect like other antiferromagnets with a nontrivial magnetic structure.

$S_{yx}(0)$ rapidly changes sign by cooling to below 20 K, strongly deviating from an approximately linear temperature dependence observed for $S_{yx}(H_{c1})$. Both coefficients vanish toward zero temperature due to Nernst's theorem[38]. The sign change of $S_{yx}(0, T)$ occurs at the same temperature where we observe a decrease of $M_R(0)$, in contrast to $\Delta M(H_{c1})$ which appears more like a magnetically saturated state at low temperatures, see Fig. 3b. While the vanishing $\sigma_{xy}(0)$ and reduced $M_R(0)$ could be considered as indications for the reformation of antiferromagnetic domains, this cannot explain the reappearance of a positive $S_{yx}(0)$ below 20 K supporting the idea of a weak modification of the magnetic structure at low temperatures.

The transverse thermoconductivity, i.e., the transverse Peltier coefficient, can be calculated in zero magnetic field by

$$\alpha_{yx} = S_{yx}\sigma_{xx} + S_{xx}\sigma_{yx} \tag{2}$$

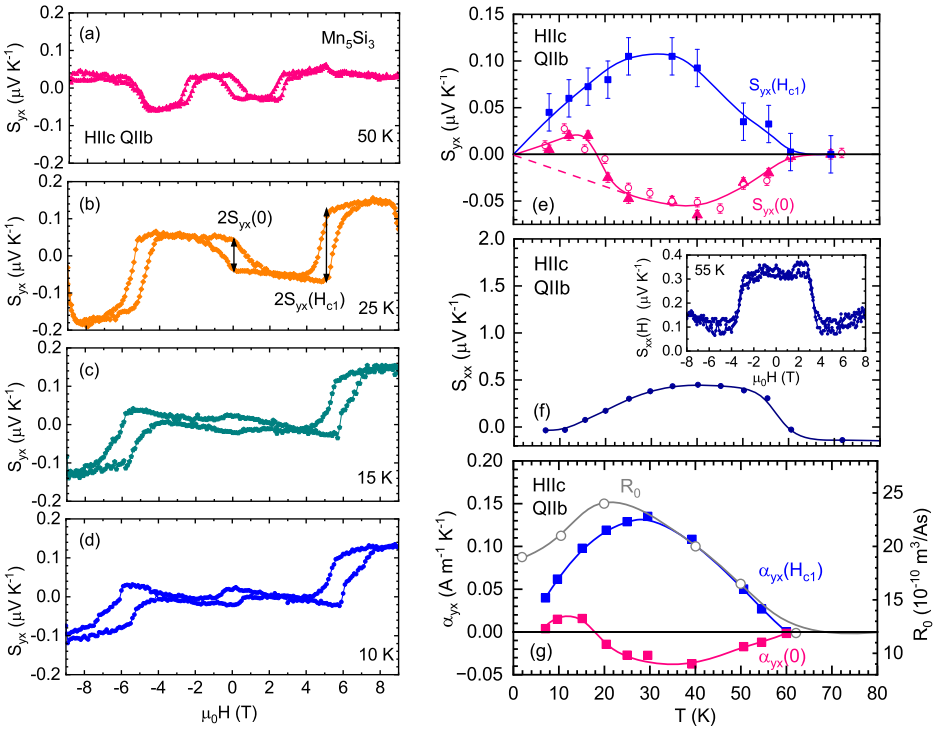

Fig. 5 | Anomalous Nernst effect of Mn_5Si_3. **a**–**d** $S_{yx}(H)$ for various temperatures with the magnetic field H applied along the crystallographic c axis. **e** $S_{yx}(0)$ and $S_{yx}(H_{c1})$ vs temperature T. Solid symbols indicate data taken from individual $S_{yx}(H)$ sweeps, see panels **a**–**d**. Open circles were calculated from the difference between $S_{yx}(H)$ measured in two consecutive temperature sweeps at positive or negative remanence. The accuracy with which the values from $S_{yx}(H)$ loops could be determined is indicated by error bars. Dashed line indicates a linear behavior toward zero temperature. **f** Temperature dependence of the Seebeck coefficient S_{xx} in zero field. Inset shows $S_{xx}(H)$ at $T = 55$ K. **g** Transverse Peltier coefficients $\alpha_{yx}(0)$ and $\alpha_{yx}(H_{c1})$ vs temperature T. Grey curve shows the ordinary Hall constant R_0 of Mn_5Si_3 thin films[18].

Here, $S_{xx} = \Delta V_x/\Delta T_x$ is the Seebeck coefficient measured in the same setup and plotted in Fig. 5f for different temperatures using $\sigma_{yx} = -\sigma_{xy}$.

An interesting detail is the magnetic field behavior of $S_{xx}(H)$ in the inset of Fig. 5f. At magnetic fields below H_{c2} the Seebeck coefficient is almost independent of H but precipituously drops at H_{c2} when crossing the phase boundary between the field-induced noncollinear AF1' phase and the high-field collinear AF2-like phase. This extraordinary sharp change of the magneto-Seebeck effect with magnetic field is observed only at H_{c2} where the magnetic order changes from noncollinear to collinear. It is correlated with the strong change of the magnetoresistance $\rho_{xx}(H)$ by ≈ 10 % at H_{c2} and $T = 45$ K[20]. This is expected from the Mott relation between the thermoelectric and electronic conductivity

$$\alpha_{xx} = \sigma_{xx} S_{xx} = \frac{\pi^2 k_B^2}{3e} T \left(\frac{\partial \sigma_{xx}}{\partial E}\right)_{\mu}. \quad (3)$$

where k_B is the Boltzmann constant, e the electron charge, and μ the electrochemical potential. It has been shown previously that the Mott relation between σ_{xx} and α_{xx} can also be applied for the transverse coefficient α_{yx}[12,43,44]

$$\alpha_{yx} = -\alpha_{xy} = -\frac{\pi^2 k_B^2}{3e} T \left(\frac{\partial \sigma_{xy}}{\partial E}\right)_{\mu}. \quad (4)$$

The transverse coefficient α_{yx} [Fig. 5g] obtained from Eq. (2) essentially shows the same behavior as $S_{yx}(0)$ [Fig. 5e]. Since $|S_{xx}\sigma_{xy}| \ll |S_{yx}\sigma_{xx}|$, α_{yx} is dominated by $S_{yx}\sigma_{xx}$ (Eq. (2)). Hence, the ANE mostly arises from the transverse heat flow (90 %) and the sign change of α_{yx} occurs due to the sign change of S_{yx}.

For Mn_5Si_3, maximum values $|S_{yx}(0)| = 0.05\ \mu VK^{-1}$ and $|S_{yx}(H_{c1})| = 0.11\ \mu VK^{-1}$ are reached at magnetizations $M_R(0) = 0.028\ \mu_B$/f.u. and $M_R(H_{c1}) = 0.17\ \mu_B$/f.u., respectively. Note that the values of $|S_{yx}(0)|$ and $|S_{yx}(H_{c1})|$ should be considered as lower limits due to the thermal resistances between the sample holder and the single crystal which give rise to a lower applied thermal gradient in the crystal than the measured $\Delta T_x = T_h - T_c$. Hence, an even larger $|S_{yx}|$ derived from the low magnetization is expected. Similar values $|S_{yx}| = 0.6\ \mu VK^{-1}$ and $\mu_0 M = 1$ mT (corresponding to $M = 0.01\ \mu_B$/f.u.) have been reported for chiral Mn_3Sn[14]. Compared to ferromagnetic metals, $|S_{yx}|$ of Mn_5Si_3 is strongly enhanced outside the broad range for which $|S_{yx}| \propto M$ is observed, in close vicinity to values of the chiral antiferromagnets Mn_3Sn[14,41] and Mn_3Ge[15,41].

In various topological magnets, the ratio $|\alpha_{xy}/\sigma_{xy}|$ increases with temperature from 1 μV/K and often approaches $k_B/e = 86\ \mu$V/K at room temperature or above[10,11,45] and thus follows a universal scaling[46], with the exception of $UCo_{0.8}Ru_{0.2}Al$ which exhibits a colossal ANE[47]. In the present case, maximum values of $|\alpha_{yx}(0)/\sigma_{xy}(0)| = 3.5\ \mu$V/K and $|\alpha_{yx}(H_{c1})/\sigma_{xy}(H_{c1})| = 5.8\ \mu$V/K are obtained for $T = 40$ K, which are only somewhat smaller when compared to values of other topological materials at this low temperature[10,11,45]. The similar ratios obtained in the AF1 and AF1' phases of Mn_5Si_3 support the correlation between the two properties α_{yx} and σ_{xy} that are predominated by intrinsic effects of the Berry curvature in both magnetic phases.

If the Berry curvature $\Omega_{n,z}(\boldsymbol{k})$ is known, the intrinsic contributions to α_{yx} and σ_{xy} can be obtained from refs. 12,13,41

$$\alpha_{yx} = -\alpha_{xy} = -\frac{e}{T\hbar} \sum_n \int \frac{d\boldsymbol{k}}{(2\pi)^3} \Omega_{n,z}(\boldsymbol{k}) g_{n,\boldsymbol{k}} \quad (5)$$

$$g_{n,\boldsymbol{k}} = (E_{n,\boldsymbol{k}} - \mu) f_{n,\boldsymbol{k}} + k_B T \left[1 + \exp\left(-\tfrac{E_{n,\boldsymbol{k}} - \mu}{k_B T}\right)\right]$$

$$\sigma_{xy} = -\frac{e^2}{\hbar} \sum_n \int \frac{d\boldsymbol{k}}{(2\pi)^3} \Omega_{n,z}(\boldsymbol{k}) f_{n,\boldsymbol{k}} \quad (6)$$

where $\boldsymbol{k} = (k_x, k_y, k_z)$ is the three-dimensional crystal momentum, $E_{n,\boldsymbol{k}}$ is the energy of the band of index n, and $f_{n,\boldsymbol{k}}$ is the Fermi-Dirac distribution function.

Finally, we argue that it is unlikely that the magnetocrystalline anisotropy is the origin of the anisotropic behaviour of both thermal effects. In the AF1 phase, nonzero AHE and ANE values are observed at zero field only for H oriented parallel to the c axis but not along the a or b axes, see Fig. 6 and ref. 19, where the latter is the magnetic easy axis in the AF1 phase[30].

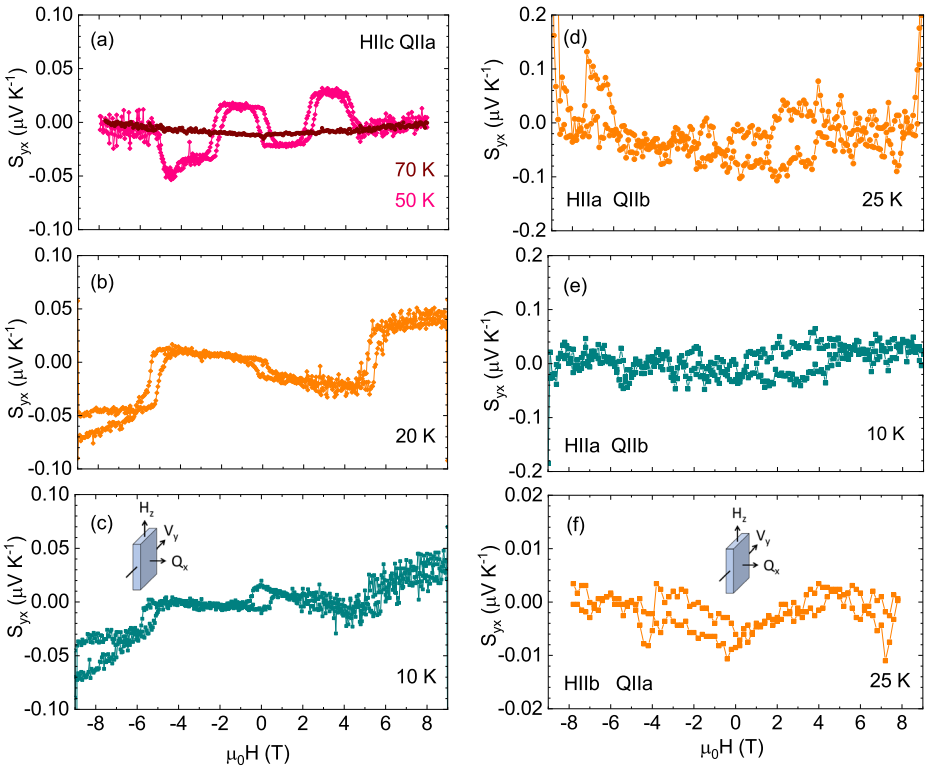

Fig. 6 | Orientation dependence of the anomalous Nernst effect. $S_{yx}(H)$ of another Mn_5Si_3 single crystal for magnetic fields H and heat flows Q applied along different crystallographic directions a, b, or c. **a**–**c** H along c, Q along the orthorhombic a direction over a length of 0.52 mm. **d**, **e** H applied along the orthorhombic a direction, Q along the orthorhombic b direction over a length of 1.2 mm. **f** H along the orthorhombic b direction, Q along the orthorhombic a direction over a length of 0.52 mm.

Discussion

Temperature dependence of the ANE

The ANE represented by S_{yx} or α_{yx} is a Fermi surface property (Eq. (5)). A sign change of these parameters at 20 K inevitably means that they reach zero around 20 K. Hence, from Eq. (4) it follows that $(\frac{\partial\sigma_{xy}}{\partial E})_{\mu} = 0$, i.e., $\sigma_{xy}(E)$ has a maximum or minimum at the Fermi surface which is shifting through the Fermi level with increasing temperature from below 20 K to above 20 K. A change of the Fermi surface at low temperatures can be also inferred from the variation of the ordinary Hall effect of Mn_5Si_3 thin films[18]. In that case, the ordinary Hall effect $\rho_{yx}^0 = R_0\mu_0 H$ could be separated from the measured signal, revealing a change of the ordinary Hall constant R_0 or the effective charge carrier density n_H with temperature and a maximum (minimum) of R_0 (n_H) around 20 K, see Fig. 5g. At this point, ab initio calculations of the electronic bandstructure and σ_{xy} are necessary for a more quantitative analysis of the AHE and ANE following the Berry-phase concept by application of Eqs. (5) and (6). Such calculations involve a knowledge of the correct magnetic configuration in the ground state of bulk Mn_5Si_3, which has not been determined so far.

A sign change of the ANE with temperature was reported earlier for the ferromagnetic semiconductor $Ga_{1-x}Mn_xAs$ and was attributed to the scattering-independent nature of the intrinsic AHE following a behavior $\rho_{yx} \propto \rho_{xx}^2$ [44]. The sign change of S_{yx} was found to be correlated with a sharp maximum in S_{xx} thus compensating this contribution to the transverse coefficient α_{yx} which did not change sign. In contrast, for Mn_5Si_3 the sign change occurs for S_{yx} *and* α_{yx} but not for S_{xx}. An analysis of the temperature dependence of α_{xy} based on the power law $\rho_{yx}^{AHE} = \lambda M_z \rho_{xx}^n$ [44] is not possible because λ of Mn_5Si_3 is strongly temperature dependent[18] in contrast to itinerant ferromagnets where it is usually temperature independent at low temperatures.

In the pyrochlore molybdate $R_2Mo_2O_7$ (R = Nd, Sm) with noncoplanar spin structure the variations of S_{xy} and α_{xy} were attributed to a contribution from the spin chirality of the system which was considered to be responsible for an enhanced AHE and a positive ANE at low temperatures[48]. A strong magnetic field reduces the amplitude of the spin chirality by aligning the Mn moments along the magnetic field direction leading to a reduced σ_{xy} and α_{xy}. It is interesting to note that this is observed only for R = Nd, Sm with non-coplanar spin structure and not for collinearly ordered $Gd_2Mo_2O_7$. In the present case, it is therefore conceivable that a similar behavior occurs due to a small change of the spin structure by moment reorientation and decrease of chirality/noncollinearity at small magnetic fields.

We only mention that for the Weyl semimetal $Co_3Sn_2S_2$ different behaviors of α_{yx} have been reported[45,49,50]. In these cases, however, S_{xy} did not change its sign with the temperature.

Below T_{N1} = 60 K, $\alpha_{yx}(H_{c1})$ first increases with decreasing temperature together with a concomitant increase of $\Delta M(H_{c1})$, eventually saturates and then decreases towards low temperatures. This is similar to the behavior of an itinerant ferromagnet and due to the dominant T-linear term in Eq. (4) after saturation of M[38]. In contrast, in the AF1 phase below H_{c1} the ANE strongly deviates from this behavior at temperatures below ≈ 20 K. We speculate that the reduction of $M_R(0)$ and the simultaneous sign changes of $\alpha_{yx}(H_{c1})$ and $S_{yx}(0)$ with temperature could arise from the different compensation of opposed Mn moments. In this respect it bears some similarity to the magnetization behavior of garnets or rare-earth transition-metal ferrimagnets below and above the compensation point.

Symmetry analysis

To gain further insights into the low-temperature behavior of Mn_5Si_3, we analyze the symmetries of the anomalous Hall and Nernst effects under a small external magnetic field. The Onsager relations establish strong symmetry requirements for each response tensor. The (thermo-)electric responses measured in our experiments are approximately odd under the reversion of a small external magnetic field (Figs. 3 and 5). Up to second order, the only odd-in-field transverse electric (thermo-electric) responses are the intrinsic and quadratic anomalous Hall (Nernst) effects[51]. These response tensors are even under space inversion $\mathcal{P}$ and odd under the combined time reversal and lattice translation symmetry $\mathcal{T}\boldsymbol{t}$[51,52]. According

to Neumann's principle, the transport coefficients must also be invariant under all the symmetries of the material. In the next paragraph, we combine the implications of the Onsager relations with Neumann's principle to investigate the symmetry constraints of the AHE and ANE in the antiferromagnetic phases AF1 and AF2 of Mn_5Si_3 (Fig. 2).

Consider the collinear AF2 phase shown in Fig. 2a. The system is invariant under both $\mathcal{P}$ and $\mathcal{T}\boldsymbol{t}$. Because the response tensors are also invariant under $\mathcal{P}$, this symmetry operation does not impose any constraint. On the other hand, the $\mathcal{T}\boldsymbol{t}$ invariance of the system imposes that the response coefficients be even under time reversal. Since the Onsager relations require the response tensors to be odd under $\mathcal{T}$, the intrinsic and quadratic anomalous Hall/Nernst effects are prohibited in the AF2 phase, in agreement with our experimental results for 60 K $< T <$ 100 K [Figs. 3h and 5e, g][18–20]. Although a neutron-diffraction study on polycrystalline Mn_5Si_3 in the AF2 phase suggested a spin canting of up to 8° toward the *b* axis for the spins still confined in the *a*-*b* plane due to Dzyaloshinskii-Moriya interaction, this would still preserve $\mathcal{P}$ and $\mathcal{T}\boldsymbol{t}$ symmetry with vanishing Hall and Nernst effects[17,29].

As mentioned above, the magnetic configurations of Mn_5Si_3 for $T < 60$ K are still under discussion[28]. The AF1 phases shown in Fig. 2b and c break $\mathcal{P}$ but (as well as other proposals in the literature) are invariant under $\mathcal{T}\boldsymbol{t}$, which allows for a p-wave non-relativistic spin splitting of the energy bands[53]. However, even though the bands are not spin-degenerate, the $\mathcal{T}\boldsymbol{t}$ symmetry prohibits the anomalous responses. We conclude that, due to $\mathcal{T}\boldsymbol{t}$ invariance, none of the proposed AF1 phases can explain our experimental signals. This suggests a slight tilting of the magnetic state for $T < 60$ K, which breaks the combined $\mathcal{T}\boldsymbol{t}$ symmetry.

The question is whether this could be caused by a residual strain in the single crystal similar to epitaxially strain prevailing in Mn_5Si_3 films[32,35,36]. Strain caused by Cu impurities was presumably responsible for generating additional magnetic phases in Mn_5Si_3 single crystals[31]. Uniaxial residual stress was reported to cause a change of the antiferromagnetic structure of polycrystalline Mn_3Sn from non-collinear and coplanar to non-coplanar[54]. In the present case, where the different phases observed in the electronic transport measurements agree with the results from neutron-diffraction experiments on different single crystals, it is unlikely that the residual stress in the crystal only evolves along the *c* axis to generate a nonzero AHE and ANE. The samples were not clamped in the ANE device with pressure [Fig. 4c] but only glued to the Cu banks of which the hot end was always freely suspended. ANE measurements shown in Figs. 5 and 6 with the magnetic field along the *c* axis were done on different samples with *c* oriented perpendicular to the plane or in the plane of the sample plate, respectively. Moreover, the strong variation of the ANE and the sign change in a small range of temperature around 20 K is even more unlikely as being due to strain. Thus, we believe that residual strain cannot explain the appearance of a finite AHE and ANE in contrast to what is expected from the symmetry analysis.

Possible deviations from the stoichiometry must always be considered. It has been previously reported that large displacements of Mn atoms from their high-symmetry positions lower the structural symmetry in Mn_3SnN or Mn_3GaN resulting in spin canting and allowing the observation of non-vanishing AHE[55]. We cannot completely rule out such effects but emphasize that an x-ray analysis of a pulverized piece from the ingot sample yielded lattice parameters that deviate less than 0.1 % from recently published data of a polycrystal[17,20].

We conclude that the reduction in the magnitude of the anomalous Hall conductivity and sign change of the anomalous Nernst conductivity below $T \leq 20$ K hints to either a new phase or a weak rearrangement of the spins due to magnetic frustration or magnetic anisotropies, as pointed out by N. Biniskos et al.[28].

Conclusion

The anomalous Nernst effect of Mn_5Si_3 single crystals displays characteristic variations with magnetic field and temperature in agreement with the magnetic-field induced transitions between different antiferromagnetic phases. The anomalous Hall effect, and Nernst effect are sizeable in the the remanent state, i.e., in absence of a magnetic field. Detailed analysis of the low-temperature behavior below 25 K shows that the anomalous Nernst effect, anomalous Hall conductivity, and magnetization in low magnetic fields exhibit an unusual temperature dependence hinting a subtle modification of the magnetic structure in the AF1 phase. Furthermore, the experimentally observed Hall and Nernst effects in the noncollinear AF1 phase are in contrast to a symmetry analysis of the proposed magnetic AF1 structures, according to which these effects should disappear. These results should be taken into account in a refined model of the magnetic structure. While first ab initio calculations of the electronic band structure and Berry curvature have been performed for the collinear magnetic phase observed in thin films[32,33], the behavior of the AHE and ANE in the non-collinear AF1 phase of Mn_5Si_3 at low temperatures is not yet fully understood and requires further investigation.

Methods

Mn_5Si_3 single crystals were obtained by a combined Bridgman and flux-growth technique and were characterized by X-ray diffraction as described earlier[20]. The single crystals have been polished and oriented by Laue diffraction, Fig. 4a, b. Magnetization data were obtained in a superconducting-quantum-interference device (SQUID) equipped with a 5 T superconducting magnet and in a vibrating sample magnetometer (VSM) with a 12 T magnet. Measurements of the AHE were performed in a physical-property measurement system (PPMS) as described in ref. 20 with 50-μm Pt wires attached to the crystal in an appropriate fashion with conductive silver-epoxy. The ANE was obtained on the same Mn_5Si_3 single crystal of thickness $t = 0.6$ mm and lengths $l_x = 1.2$ mm and $l_y = 1.4$ mm along *z*, *x*, and *y*, respectively. The crystal was mounted between two Cu clamps electrically isolated by 20-μm Kapton foil and a resistor R_H was attached on one clamp serving as a heater generating a temperature difference $\Delta T_x = T_h - T_c$ between the hot and cold side, inset Fig. 4c. Both temperatures were determined by using calibrated resistive thermometers. The power of the heater was always adjusted to keep ΔT_x below 10% of the average temperature $T_0 = (T_h + T_c)/2$. The Nernst voltage ΔV_y was measured along the *y* direction with a nanovoltmeter. The crystal was mounted with the crystallographic *a*, *b*, and *c* axes oriented parallel to the *y*, *x*, and *z* directions, respectively, with the heat flow *Q* along the *b* axis and the magnetic field oriented along the *c* axis, Fig. 4c.

Data availability

The data that support the findings of this study are available in the KITopen repository with the identifier https://doi.org/10.35097/XqLocxHPRfSlZYQh.

Received: 8 May 2024; Accepted: 16 August 2024;
Published online: 30 August 2024

References

1. Jungwirth, T., Marti, X., Wadley, P. & Wunderlich, J. Antiferromagnetic spintronics. *Nat. Nanotech.* **11**, 231 (2016).
2. Baltz, V. et al. Antiferromagnetic spintronics. *Rev. Mod. Phys.* **90**, 015005 (2018).
3. Nagaosa, N., Sinova, J., Onoda, S., MacDonald, A. H. & Ong, N. P. Anomalous Hall effect. *Rev. Mod. Phys.* **82**, 1539–1592 (2010).
4. Machida, Y., Nakatsuji, S., Onoda, S., Tayama, T. & Sakakibara, T. Time-reversal symmetry breaking and spontaneous Hall effect without magnetic dipole order. *Nature* **463**, 210–213 (2010).
5. Chen, H., Niu, Q. & MacDonald, A. Anomalous Hall effect arising from noncollinear antiferromagnetism. *Phys. Rev. Lett.* **112**, 017205 (2014).
6. Kübler, J. & Felser, C. Non-collinear antiferromagnets and the anomalous Hall effect. *EPL* **108**, 67001 (2014).
7. Nakatsuji, S., Kiyohara, N. & Higo, T. Large anomalous Hall effect in a non-collinear antiferromagnet at room temperature. *Nature* **527**, 212–215 (2015).

8. Kiyohara, N., Tomita, T. & Nakatsuji, S. Giant anomalous hall effect in the chiral antiferromagnet Mn_3Ge. *Phys. Rev. Appl.* **5**, 064009 (2016).
9. Nayak, A. K. et al. Large anomalous Hall effect driven by a nonvanishing Berry curvature in the noncolinear antiferromagnet Mn_3Ge. *Sci. Adv.* **2**, e1501870 (2016).
10. Li, X. et al. Anomalous Nernst and Righi-Leduc effects in Mn_3Sn Berry curvature and entropy flow. *Phys. Rev. Lett.* **119**, 056601 (2017).
11. Xu, L. et al. Finite-temperature violation of the anomalous transverse Wiedemann-Franz law. *Sci. Adv.* **6**, eaaz3522 (2020).
12. Xiao, D., Yao, Y., Fang, Z. & Niu, Q. Berry-phase effect in anomalous thermoelectric transport. *Phys. Rev. Lett.* **97**, 026603 (2006).
13. Xiao, D., Chang, M.-C. & Niu, Q. Berry phase effects on electronic properties. *Rev. Mod. Phys.* **82**, 1959–2007 (2010).
14. Ikhlas, M. et al. Large anomalous Nernst effect at room temperature in a chiral antiferromagnet. *Nat. Phys.* **13**, 1085 (2017).
15. Wuttke, C. et al. Berry curvature unravelled by the anomalous Nernst effect in Mn_3Ge. *Phys. Rev. B* **100**, 085111 (2019).
16. Hong, D. et al. Large anomalous Nernst and inverse spin-Hall effects in epitaxial thin films of kagome semimetal Mn_3Ge. *Phys. Rev. Mater.* **4**, 094201 (2020).
17. Gottschilch, M. et al. Study of the antiferromagnetism of Mn_5Si_3: an inverse magnetocaloric effect material. *J. Mater. Chem.* **22**, 15275 (2012).
18. Sürgers, C., Fischer, G., Winkel, P. & Löhneysen, H. V. Large topological Hall effect in the non-collinear phase of an antiferromagnet. *Nat. Commun.* **5**, 3400 (2014).
19. Sürgers, C., Kittler, W., Wolf, T. & Löhneysen, H. V. Anomalous Hall effect in the noncollinear antiferromagnet Mn_5Si_3. *AIP Adv.* **6** https://pubs.aip.org/aip/adv/article/6/5/055604/998720/Anomalous-Hall-effect-in-the-noncollinear (2016).
20. Sürgers, C. et al. Switching of a large anomalous Hall effect between metamagnetic phases of a non-collinear antiferromagnet. *Sci. Rep.* **7**, 42982 (2017).
21. Biniskos, N. et al. Spin fluctuations drive the inverse magnetocaloric effect in Mn_5Si_3. *Phys. Rev. Lett.* **120**, 257205 (2018).
22. Das, S. C., Mandal, K., Dutta, P., Pramanick, S. & Chatterjee, S. Observation of inverted hysteresis loop and thermomagnetic irreversibility in the antiferromagnetic Mn_5Si_3 alloy. *Phys. Rev. B* **100**, 024409 (2019).
23. Lander, G. H., Brown, P. J. & Forsyth, J. B. The antiferromagnetic structure of Mn_5Si_3. *Proc. Phys. Soc.* **91**, 332–340 (1967).
24. Brown, P. J. & Forsyth, J. B. Antiferromagnetism in Mn_5Si_3: the magnetic structure of the AF2 phase at 70 K. *J. Phys.: Condens. Matter* **7**, 7619–7628 (1995).
25. Silva, M. R., Brown, P. J. & Forsyth, J. B. Magnetic moments and magnetic site susceptibilities in Mn_5Si_3. *J. Phys. Condens. Matter* **14**, 8707–8713 (2002).
26. Brown, P. J., Forsyth, J. B., Nunez, V. & Tasset, F. The low-temperature antiferromagnetic structure of Mn_5Si_3 revised in the light of neutron polarimetry. *J. Phys.: Condens. Matter* **4**, 10025–10036 (1992).
27. Bilbao. Crystallographic Server http://webbdcrista1.ehu.es/magndata, No. 1.307.
28. Biniskos, N. et al. Complex magnetic structure and spin waves of the noncollinear antiferromagnet $Mn_5 Si_3$. *Phys. Rev. B* **105**, 104404 (2022).
29. dos Santos, F. J. et al. Spin waves in the collinear antiferromagnetic phase of Mn_5Si_3. *Phys. Rev. B* **103**, 024407 (2021).
30. Biniskos, N. et al. An overview of the spin dynamics of antiferromagnetic Mn_5Si_3. *APL Mater.* **11**, 081103 (2023).
31. Luccas, R. F. et al. Magnetic phase diagram, magnetotransport and inverse magnetocaloric effect in the noncollinear antiferromagnet Mn_5Si_3. *J. Magn. Magn. Mater.* **489**, 165451 (2019).
32. Reichlova, H. et al. Observation of a spontaneous anomalous Hall response in the Mn_5Si_3 d-wave altermagnet candidate. *Nat. Commun.* **15**, 4961 (2024).
33. Šmejkal, L., Hellenes, A. B., González-Hernández, R., Sinova, J. & Jungwirth, T. Giant and tunneling magnetoresistance in unconventional collinear antiferromagnets with nonrelativistic spin-momentum coupling. *Phys. Rev. X* **12**, 011028 (2022).
34. Šmejkal, L., Sinova, J. & Jungwirth, T. Beyond conventional ferromagnetism and antiferromagnetism: a phase with nonrelativistic spin and crystal rotation symmetry. *Phys. Rev. X* **12**, 031042 (2022).
35. Badura, A. et al. Observation of the anomalous Nernst effect in altermagnetic candidate Mn_5Si_3 http://arxiv.org/abs/2403.12929 (2024).
36. Han, L. et al. Electrical 180° switching of Néel vector in spin-splitting antiferromagnet. *Sci. Adv.* https://www.science.org/doi/10.1126/sciadv.adn0479 (2024).
37. Han, L. et al. Observation of non-volatile anomalous Nernst effect in altermagnet with collinear Néel vector http://arxiv.org/abs/2403.13427 (2024).
38. Miyasato, T. et al. Crossover behavior of the anomalous Hall effect and anomalous Nernst effect in itinerant ferromagnets. *Phys. Rev. Lett.* **99**, 086602 (2007).
39. Onoda, S., Sugimoto, N. & Nagaosa, N. Quantum transport theory of anomalous electric, thermoelectric, and thermal Hall effects in ferromagnets. *Phys. Rev. B* **77**, 165103 (2008).
40. Lee, M., Onose, Y., Tokura, Y. & Ong, N. P. Hidden constant in the anomalous Hall effect of high-purity magnet MnSi. *Phys. Rev. B* **75**, 172403 (2007).
41. Chen, T. et al. Anomalous transport due to Weyl fermions in the chiral antiferromagnets Mn_3X, X = Sn, Ge. *Nat. Commun.* **12**, 572 (2021).
42. Vinokurova, L., Ivanov, V., Kulatov, E. & Vlasov, A. Magnetic phase transitions and electronic structure of the manganese silicides. *J. Magn. Magn. Mater.* **90-91**, 121–125 (1990).
43. Wang, Y. et al. Onset of the vortexlike Nernst signal above T_c in $La_{2-x}Sr_xCuO_4$ and $Bi_2Sr_{2-y}La_yCuO_6$. *Phys. Rev. B* **64**, 224519 (2001).
44. Pu, Y., Chiba, D., Matsukura, F., Ohno, H. & Shi, J. Mott relation for anomalous hall and Nernst effects in $Ga_{1-x}Mn_xAs$ ferromagnetic semiconductors. *Phys. Rev. Lett.* **101**, 117208 (2008).
45. Ding, L. et al. Intrinsic anomalous Nernst effect amplified by disorder in a half-metallic semimetal. *Phys. Rev. X* **9**, 041061 (2019).
46. Xu, L. et al. Anomalous transverse response of Co_2MnGa and universality of the room-temperature $\alpha_{ij}^A/\sigma_{ij}^A$ ratio across topological magnets. *Phys. Rev. B* **101**, 180404 (2020).
47. Asaba, T. et al. Colossal anomalous Nernst effect in a correlated noncentrosymmetric kagome ferromagnet. *Sci. Adv.* https://www.science.org/doi/10.1126/sciadv.abf1467 (2021).
48. Hanasaki, N. et al. Anomalous Nernst effects in pyrochlore molybdates with spin chirality. *Phys. Rev. Lett.* **100**, 106601 (2008).
49. Guin, S. N. et al. Zero-field Nernst effect in a ferromagnetic Kagome-Lattice Weyl-Semimetal $Co_3Sn_2S_2$. *Adv. Mater.* **31**, 1806622 (2019).
50. Yang, H. et al. Giant anomalous Nernst effect in the magnetic Weyl semimetal $Co_3Sn_2S_2$. *Phys. Rev. Mater.* **4**, 024202 (2020).
51. Grimmer, H. Thermoelectric transport properties in magnetically ordered crystals. *Acta Cryst. A* **73**, 333–345 (2017).
52. Šmejkal, L., González-Hernández, R., Jungwirth, T. & Sinova, J. Crystal time-reversal symmetry breaking and spontaneous Hall effect in collinear antiferromagnets. *Sci. Adv.* **6** https://doi.org/10.1126/sciadv.aaz8809 (2020).
53. Hellenes, A. B., Jungwirth, T., Sinova, J. & Šmejkal, L. Unconventional p-wave magnets http://arxiv.org/abs/2309.01607 (2024).
54. Deng, J. J. et al. Effect of residual strain on magnetic properties and Hall effect in chiral antiferromagnet Mn_3Sn. *J. Phys. D: Appl. Phys.* **55**, 275001 (2022).

55. Rimmler, B. H. et al. Atomic displacements enabling the observation of the anomalous Hall effect in a non-collinear antiferromagnet. *Adv. Mater.* **35**, 2209616 (2023).
56. Gallego, S. V. et al. MAGNDATA: towards a database of magnetic structures. II. The incommensurate case. *J. Appl Cryst.* **49**, 1941–1956 (2016).

Acknowledgements

We thank N. Biniskos for helpful discussions. This work was supported by the Deutsche Forschungsgemeinschaft (DFG) through CRC TRR 288 - 422213477 “ElastoQMat” (Projects A08, A09). We acknowledge support by the KIT-Publication Fund of the Karlsruhe Institute of Technology.

Author contributions

C.S. conceived the experiments and carried out the electronic transport measurements. G.F. measured the magnetization. W.H.C., A.B.H., L. Š., and J. S. contributed to the theory and symmetry analysis. M. M. performed the Laue measurements. T. Wolf grew the single crystals. C.S., W.H.C., M.M. and W.W. analyzed the data and wrote the manuscript.

Funding

Open Access funding enabled and organized by Projekt DEAL.

Competing interests

The authors declare no competing interests.

Additional information

Supplementary information The online version contains supplementary material available at https://doi.org/10.1038/s43246-024-00617-x.

Correspondence and requests for materials should be addressed to Christoph Sürgers.

Peer review information *Communications Materials* thanks Mingquan He, Cheng Song and the other, anonymous, reviewer(s) for their contribution to the peer review of this work. Primary Handling Editors: Xiaokang Li and Aldo Isidori. A peer review file is available.